Optimal Task-Invariant Energetic Control for a Knee-Ankle Exoskeleton

Jianping Lin, *Student Member, IEEE*, Nikhil V. Divekar, *Student Member, IEEE*, Ge Lv, *Member, IEEE*, Robert D. Gregg, *Senior Member, IEEE*

***Abstract*— Task-invariant control methods for powered exoskeletons provide flexibility in assisting humans across multiple activities and environments. Energy shaping control serves this purpose by altering the human body's dynamic characteristics in closed loop. Our previous work on potential energy shaping alters the gravitational vector to reduce the user's perceived gravity, but this method cannot provide velocity-dependent assistance. The interconnection and damping assignment passivity-based control (IDA-PBC) method provides more freedom to shape a dynamical system's energy through the interconnection structure of a port-controlled Hamiltonian system model. This paper derives a novel energetic control strategy based on IDA-PBC for a backdrivable knee-ankle exoskeleton. The control law provides torques that depend on various basis functions related to gravitational and gyroscopic terms. We optimize a set of constant weighting parameters for these basis functions to obtain a control law that produces able-bodied joint torques during walking on multiple ground slopes. We perform experiments with an able-bodied human subject wearing a knee-ankle exoskeleton to demonstrate reduced activation in certain lower-limb muscles.**

***Index Terms*— Biomedical, Optimization, Robotics**

I. Introduction

COMMERCIALIZED exoskeletons such as HAL, ReWalk, Ekso Bionics, and Wandercraft use trajectory-based, kinematic control methods for specific tasks [1], [2]. This type of control is appropriate for paraplegia, where the exoskeleton provides complete assistance. However, it overly constrains the volitional motion of people with remnant voluntary ability, e.g., stroke patients. In contrast, trajectory-free control methods are now being developed to provide task-invariant assistance for practicing/relearning leg motions or performing a continuum of activities in varying environments.

The energy shaping method provides task-invariant control by altering the human body's dynamic characteristics in the closed-loop system. Lv and Gregg [3] proposed the potential energy shaping for the underactuated human-exoskeleton system based on the controlled Lagrangians method [4]. They proved the system's passivity and stability properties for the fully-actuated contact condition, but these proofs could not be extended to underactuated phases because of the lack of a well-defined potential energy in closed loop. Two different forms of potential energy shaping were experimentally implemented on a powered knee-ankle exoskeleton in [5], [6]. By also shaping the mass/inertia matrix in the closed-loop system, total energy shaping can achieve greater assistance than potential energy shaping alone in simulation [7]. However, the corresponding controller requires complicated calculations of the inverse of the mass/inertia matrix, which has practical challenges for real-time implementation. In [8], we combined a well-defined, closed-loop modified potential energy (MPE) with virtual spring and damping energy as an indirect form of total energy shaping (i.e., kinetic terms corresponding to the velocity-dependent damping energy), which achieved passivity and stability during all contact conditions. However, the passivity condition [9], where the physical damping in the mechanism must be sufficient to dissipate the excess energy due to the sampling in discrete-time control implementations in embedded systems, limited the overall shaping of the kinetic terms. This method failed to achieve significant results over potential energy shaping.

Interconnection and damping assignment passivity-based control (IDA-PBC) provides extra freedom to shape the internal interconnection structure of a port-controlled Hamiltonian system model [10], [11], which allows the shaping of inertial terms, gravitational terms, and gyroscopic terms (including centrifugal and Coriolis forces). This method has been used to generate robust gaits for an underactuated compass-like biped robot [12]. The present paper applies this method to resolve current challenges for task-invariant exoskeleton control, including the inertia matrix inverse, proofs of passivity and stability, and invariant contact conditions.

This paper presents a novel energetic control strategy based on the IDA-PBC method for a backdrivable knee-ankle exoskeleton designed in [5]. The contributions are summarized as follows. First, the new control law provides torques based on a linear combination of designed basis functions corresponding to gravitational force vectors and gyroscopic forces. The designed basis functions enable velocity-dependent assistance, e.g., during early and late stance, which was not possible in prior implementations of potential energy shaping. Second, we formulate an optimization problem to design the basis functions' weighting parameters to fit normative biological joint torques [13] for walking on multiple ground slopes. The resulting torque control law produces a fraction of the normative joint torque profile to offload musculature as in [14],

This work was supported by the National Science Foundation under Award Number 1652514 / 1949869. Robert D. Gregg holds a Career Award at the Scientific Interface from the Burroughs Wellcome Fund.

J. Lin, N. V. Divekar, and R. D. Gregg are with the Robotics Institute, University of Michigan, Ann Arbor, MI 48109, USA. G. Lv is with the Department of Mechanical Engineering, Clemson University, Clemson, SC 29634, USA. (Correspondence: rdgregg@umich.edu)

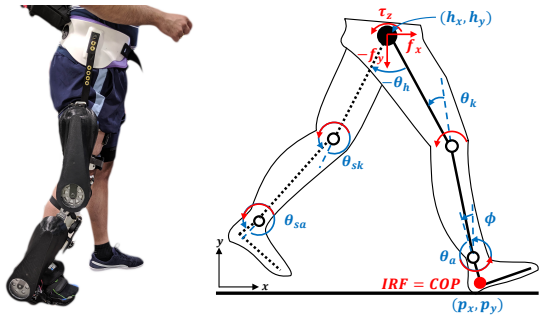

Fig. 1. Left: Comex knee-ankle exoskeleton worn by a healthy user (reproduced from [6]). Right: Kinematic model of the human body (reproduced from [8]). COP denotes Center of Pressure. The solid links denote the stance leg, and the dashed links denote the swing leg. Red arcs indicate torques.

[15], but for *multiple* tasks. Third, we assess muscular effort of one able-bodied human subject with the first experimental implementation of *total* energy shaping on an exoskeleton.

II. Modeling and Control Methods

In this section, we briefly review the Hamiltonian dynamics of the proposed human-exoskeleton system and the IDA-PBC method. In particular, we introduce sufficient and necessary conditions for the existence of a feedback control law that renders an open-loop system equivalent to another closed-loop system (a process known as *matching*).

A. Human-Exoskeleton Dynamics

The human-exoskeleton biped model is shown in Fig. 1. The Cartesian coordinates of the heel, (p_x, p_y), are defined with respect to the inertial reference frame (IRF), which depends on the contact phase. The heel angle ϕ is defined with respect to the vertical axis, and θ_a and θ_k are the stance ankle and knee angles, respectively. The angle between the stance thigh and the swing thigh is denoted by θ_h, and θ_{sk} and θ_{sa} are the swing knee and ankle angles, respectively. The masses of the human and exoskeleton are combined together.

For control purposes, the dynamics of the stance and swing legs are modeled separately with coupled interaction forces $F = [f_x, f_y, \tau_z]^T$. The 5-DOF stance leg model has the generalized coordinates $q = [p_x, p_y, \phi, \theta_a, \theta_k]^T$. The conjugate momenta $p = M(q)\dot{q}$ are defined by the positive-definite inertia matrix $M(q) \in \mathbb{R}^{5\times5}$ and the velocity vector $\dot{q}$. The dynamics can be characterized by the Hamiltonian $H(q,p) = \frac{1}{2}p^T M(q)^{-1}p + V(q)$, where $V(q)$ is the potential energy, and expressed in the port-controlled Hamiltonian form as

$$\begin{bmatrix}\dot{q}\\ \dot{p}\end{bmatrix} = \begin{bmatrix}0_{5\times5} & I_{5\times5}\\ -I_{5\times5} & 0_{5\times5}\end{bmatrix}\nabla H + \begin{bmatrix}0_{5\times1}\\ \tau + A^T\lambda\end{bmatrix}, \tag{1}$$

where the gradient $\nabla H = [(\partial_q H)^T, (\partial_p H)^T]^T$, and the vector of joint torques $\tau \in \mathbb{R}^5$ sums up the exoskeleton input $\tau_{\text{exo}} = Gu$ and the human input $\tau_{\text{hum}} = Gv + J^T F$. The control inputs $u \in \mathbb{R}^2$ and $v \in \mathbb{R}^2$ represent the exoskeleton and human torques at the knee and ankle joints, respectively. They are mapped into the overall dynamics via matrix $G \in \mathbb{R}^{5\times2}$. The system is underactuated with the number of generalized coordinates larger than the number of control inputs. The interaction forces

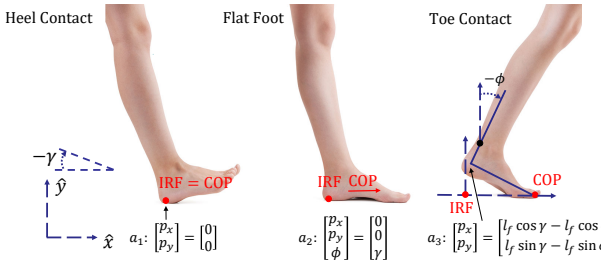

Fig. 2. Heel contact (left), flat foot (center), and toe contact (right) during the single-support period of human locomotion. The biped is assumed to be walking on a slope with angle γ. This figure is updated from [5].

F are mapped into the system's dynamics by the Jacobian matrix J. The Lagrange multiplier λ represents the ground reaction forces (GRFs) and is mapped into the system through the constraint matrix A. From now on we omit q and p terms in matrices to simplify notation.

Following [5] we incorporate holonomic contact constraints in the human-exoskeleton dynamics. The constraint functions can be expressed as $a_\ell(q) = 0_{c\times1}$, where c is the number of constraints and the subscript $\ell \in \{\text{heel}, \text{flat}, \text{toe}\}$ indicates the contact configuration as shown in Fig. 2. The constraint matrix $A = \nabla_q a_\ell \in \mathbb{R}^{c\times5} = [A_\ell \ 0_{c\times2}]$ satisfies $A\dot{q} = A\partial_p H = 0$ given the top row of (1). For the heel contact phase, the holonomic contact constraint is $a_{heel}(q) = [p_x, p_y]^T = 0$ and the matrix $A_{heel} = [I_{2\times2}, 0_{2\times1}]$. At the flat foot phase, the constraint is $a_{flat}(q) = [p_x, p_y, \phi - \gamma]^T = 0$ and the matrix $A_{flat} = I_{3\times3}$. For the toe contact phase, the constraint is $a_{toe}(q) = [p_x - l_f(\cos\gamma - \cos\phi), p_y - l_f(\sin\gamma - \sin\phi)]^T = 0$ and the matrix $A_{toe}(q) = \begin{bmatrix}1 & 0 & -l_f\sin(\phi)\\ 0 & 1 & l_f\cos(\phi)\end{bmatrix}$, where γ is the slope angle and l_f is the length of the foot. More details for the contact constraints are given in [3], [5].

For the swing leg model, the configuration vector is given by $q_{sw} = [h_x, h_y, \theta_{th}, \theta_{sk}, \theta_{sa}]^T$, where (h_x, h_y) are the positions of the hip with respect to the IRF. The angle between the vertical axis and the swing thigh is denoted as θ_{th}. The swing leg dynamics do not have contact constraints.

B. Incorporating Contact Constraints into Dynamics

We cannot directly apply the IDA-PBC method to dynamics (1) due to the varying contact conditions during stance. Our previous approaches [7], [8] treated the GRFs as the external forces and made assumptions on contact matrices to cancel out the effect of the GRFs in the control law. In this paper, we explicitly express the GRFs in the dynamics and obtain a contact-invariant control law.

We first differentiate $A\partial_p H = 0$ along q and p and plug in $\dot{q}$ and $\dot{p}$ from (1) to obtain

$$\begin{aligned}\frac{d}{dt}(A\partial_p H) &= \partial_q(A\partial_p H)^T\dot{q} + \partial_p(A\partial_p H)^T\dot{p}\\ &= \partial_q(A\partial_p H)^T\partial_p H - A\partial^2_{p^2}H(\partial_q H - \tau - A^T\lambda) = 0,\end{aligned}$$

so that λ can be solved as

$$\lambda = (A\partial^2_{p^2}HA^T)^{-1}[-\partial_q(A\partial_p H)^T\partial_p H + A\partial^2_{p^2}H(\partial_q H - \tau)].$$

Plugging λ into (1) and setting $W = (A\partial_{p^2}^2 HA^T)^{-1} \in \mathbb{R}^{c\times c}$,

$$\begin{bmatrix}\dot{q}\\ \dot{p}\end{bmatrix} = \begin{bmatrix}0 & I\\ -I + A^T WA\partial_{p^2}^2 H & -A^T W\partial_q (A\partial_p H)^T\end{bmatrix}\nabla H + \begin{bmatrix}0\\ (I - A^T WA\partial_{p^2}^2 H)(Gu + Gv + J^T F)\end{bmatrix}.$$

We can augment the above system in the port-controlled Hamiltonian form [11], where

$$\begin{bmatrix}\dot{q}\\ \dot{p}\end{bmatrix} = \mathscr{J}\nabla H + \begin{bmatrix}0\\ G_\lambda(u+v) + J_\lambda^T F\end{bmatrix}.$$

The skew-symmetric matrix $\mathscr{J} = -\mathscr{J}^T$ is defined as

$$\mathscr{J} = \begin{bmatrix}0 & X_\lambda^T\\ -X_\lambda & Y_\lambda\end{bmatrix},\ X_\lambda = I - A^T WA\partial_{p^2}^2 H,$$
$$Y_\lambda = -A^T W\partial_q (A\partial_p H)^T + \partial_q (A\partial_p H)WA,$$

where we apply $A\partial_p H = 0$ to obtain the upper-right block of the matrix $\mathscr{J}$. The matrix $\mathscr{J}$ reveals the internal interconnection structure of the open-loop dynamics, and matrices $G_\lambda = X_\lambda G$ and $J_\lambda^T = X_\lambda J^T$ are defined respectively.

C. Matching Condition with Constrained Dynamics

Assume we have closed the feedback loop for exoskeleton input u, while the human inputs v and F remain open-loop in the Hamiltonian system. We consider a desired, closed-loop Hamiltonian $\tilde{H}(p,q) = \frac{1}{2}p^T\tilde{M}^{-1}p + \tilde{V}$, where $\tilde{V} = V + \hat{V}$ represents the new potential energy with shaping term $\hat{V}$. The corresponding gravitational vector is $\tilde{N} = \nabla_q\tilde{V} = \nabla_q V + \nabla_q\hat{V} = N + \hat{N}$. We set $\tilde{M} = M$ to simplify the matching process and avoid complicated calculations of the inverse of the mass/inertia matrix in the control law. However, we will still achieve velocity-dependent shaping through the interconnection structure of the closed-loop Hamiltonian system. The desired closed-loop dynamics based on $\tilde{H}$ are

$$\begin{bmatrix}\dot{q}\\ \dot{p}\end{bmatrix} = \begin{bmatrix}0 & I\\ -I & J_2\end{bmatrix}\nabla\tilde{H} + \begin{bmatrix}0\\ Gv + J^T F + A^T\tilde{\lambda}\end{bmatrix}, \tag{2}$$

where the skew-symmetric matrix J_2 represents the extra DOF provided by the IDA-PBC method, and

$$\tilde{\lambda} = (A\partial_{p^2}^2 HA^T)^{-1}\{-\partial_q (A\partial_p H)^T\partial_p H + A\partial_{p^2}^2 H[\partial_q\tilde{H} - J_2\partial_p H - Gv - J^T F]\}.$$

Plugging $\tilde{\lambda}$ into (2), we have

$$\begin{bmatrix}\dot{q}\\ \dot{p}\end{bmatrix} = \tilde{\mathscr{J}}\nabla\tilde{H} + \begin{bmatrix}0\\ G_{\tilde{\lambda}}v + J_{\tilde{\lambda}}^T F\end{bmatrix},$$

where $\tilde{\mathscr{J}} = -\tilde{\mathscr{J}}^T = \begin{bmatrix}0 & X_{\tilde{\lambda}}^T\\ -X_{\tilde{\lambda}} & Y_{\tilde{\lambda}}\end{bmatrix}$ is a skew-symmetric matrix describing the internal interconnection structure of the closed-loop system with $X_{\tilde{\lambda}} = X_\lambda$, and $Y_{\tilde{\lambda}} = -Y_{\tilde{\lambda}}^T = J_2 - A^T W[\partial_q (A\partial_p H)^T + A\partial_{p^2}^2 HJ_2] + [J_2^T\partial_{p^2}^2 HA^T + \partial_q (A\partial_p H)]WA$. Matrices $G_{\tilde{\lambda}}$ and $J_{\tilde{\lambda}}$ are equivalent to G_λ and J_λ.

Based on standard results in [16], Hamiltonian systems (1) and (2) *match* if we have

$$G_\lambda u = -X_\lambda(\partial_q\tilde{H} - \partial_q H) + (Y_{\tilde{\lambda}} - Y_\lambda)\partial_p H,$$
$$= X_\lambda(-\partial_q\tilde{H} + \partial_q H + J_2\partial_p H),$$

which yields the corresponding *matching condition* as

$$0 = G_\lambda^\perp X_\lambda(-\partial_q\tilde{H} + \partial_q H + J_2\partial_p H), \tag{3}$$

where $G_\lambda^\perp \in \mathbb{R}^{3\times 5}$ is the (full-rank) left annihilator of G_λ, i.e., $G_\lambda^\perp G_\lambda = 0$.

To solve the matching condition (3), we express X_λ explicitly by decomposing M into four sub-matrices as

$$M = \begin{bmatrix}M_1 & M_2\\ M_2^T & M_4\end{bmatrix},$$

where $M_1 \in \mathbb{R}^{3\times 3}$ and $M_4 \in \mathbb{R}^{2\times 2}$. Then we obtain

$$M^{-1} = \begin{bmatrix}\Delta^{-1} & -\Delta^{-1}M_2M_4^{-1}\\ -M_4^{-1}M_2^T\Delta^{-1} & M_4^{-1} + M_4^{-1}M_2^T\Delta^{-1}M_2M_4^{-1}\end{bmatrix},$$

where $\Delta = M_1 - M_2M_4^{-1}M_2^T$. As a result, we have $W = (A\Delta^{-1}A^T)^{-1}$ and X_λ can be expressed as

$$X_\lambda = \begin{bmatrix}I_{3\times 3} - Z_\lambda & Z_\lambda M_2M_4^{-1}\\ 0 & I_{2\times 2}\end{bmatrix},$$

where $Z_\lambda = A_\ell^T WA_\ell\Delta^{-1}$. Plugging X_λ into G_λ, we have $G_\lambda = [M_4^{-1}M_2^T Z_\lambda^T\ \ I_{2\times 2}]^T$ and the corresponding left annihilator $G_\lambda^\perp$ equals $[I_{3\times 3}\ \ -Z_\lambda M_2M_4^{-1}]$. Plugging in $G_\lambda^\perp$ and X_λ, we have the following solution of the matching condition (3) as

$$0 = \begin{bmatrix}I_{3\times 3} - Z_\lambda & 0_{3\times 2}\end{bmatrix}[-\partial_q\tilde{H} + \partial_q H + J_2\partial_p H],$$
$$= \begin{bmatrix}I_{3\times 3} - Z_\lambda & 0_{3\times 2}\end{bmatrix}[-\tilde{N} + N + J_2M^{-1}p]. \tag{4}$$

By zeroing the unactuated parts (first three elements) of $-\tilde{N} + N + J_2M^{-1}p$, the matching condition (3) is satisfied.

The above solution is equivalent to the results in [8], where we treated the GRFs as external forces and assumed there exists a mapping of the GRFs between the open-loop and closed-loop systems. Here, we incorporate the GRFs into the system's dynamics to enable proofs of passivity and stability without making assumptions on the GRFs.

D. Shaping Strategies and Control Law

As mentioned in [8], a proper potential energy $\tilde{V}$ exists in the closed-loop system when the gravitational forces vector $\tilde{N}$ is well-defined with a symmetric Jacobian matrix, i.e., $\frac{\partial\tilde{N}_i}{\partial q_j} = \frac{\partial\tilde{N}_j}{\partial q_i}$ for any $i, j \in \{1,\cdots,5\}$. This closed-loop potential energy can then be retrieved by the variable gradient method [17], even during the underactuated phases.

The interconnection structure J_2 provides extra freedom to introduce *artificial* gyroscopic terms $Q^T\partial_p H$, where Q is a smooth vector-valued function, and $J_2 = (\partial_q Q)^T - \partial_q Q$. The artificial gyroscopic terms $Q^T\partial_p H$ are linear in the p-variables (the momenta). As mentioned in [10], $Q(q)$ must depend only on the coordinates q for the closed-loop system (2) to be integrable, i.e., there exists an equivalent Lagrangian $\tilde{L}(q,\dot{q}) = \frac{1}{2}\dot{q}^T M\dot{q} + \dot{q}^T Q(q) - \tilde{V}$ to ensure passivity. Given the solution (4), the shapeable structure of the closed-loop Hamiltonian system is characterized below.

Proposition 2.1: The closed-loop system (2) is integrable with a well-defined potential energy if the unactuated parts of $\hat{N}$ and Q are zero, and the actuated parts depend only on the actuated state variables. For the stance leg

model, this means $\hat{N} = [0,0,0,\hat{N}_4(\theta_a,\theta_k),\hat{N}_5(\theta_a,\theta_k)]^T$ and $Q = [0,0,0,Q_4(\theta_a,\theta_k),Q_5(\theta_a,\theta_k)]^T$.

The proof follows by checking the skew-symmetry property of the J_2 matrix and the symmetry of the Jacobian matrix $\partial_q \tilde{N}$ in the solution (4).

The control law with the feasible shaping structure is

$$u = G^+(\partial_q H - \partial_q \tilde{H} + J_2 M^{-1} p), \tag{5}$$

with $G^+ = (G^T G)^{-1} G^T$ being the left pseudoinverse of G. This IDA-PBC method is more general than the controller in [8] by including artificial gyroscopic terms that achieve velocity-dependent shaping without affecting the system's kinetic energy due to the skew-symmetry of J_2.

We can form multiple basis functions for the shaping terms in (5) as long as Proposition 2.1 is satisfied, which converts our controller design into an optimization process to fit the normative joint moment data in [13]. Importantly, the basis functions have physical meanings that correspond to the gravitational vector and the gyroscopic forces that act within the system, resulting in an integrable Hamiltonian system. These basis functions aim to change the effect of these forces and capture the essential characteristics of walking.

We design $\hat{N} = -\alpha_1\xi_1 - \cdots - \alpha_i\xi_i$ and $J_2 M^{-1} p = \alpha_{i+1}\xi_{i+1} + \cdots + \alpha_w\xi_w$ as linear combinations of the basis functions $\{\xi_1, \xi_2, \ldots, \xi_w\}$, where $\xi_i \in \mathbb{R}^{5\times 1}$ and w is the total number of basis functions. We express the torque control input $u = G^+(-\hat{N} + J_2 M^{-1} p) = G^+(\alpha_1\xi_1 + \alpha_2\xi_2 + \cdots + \alpha_w\xi_w) = \Phi(q,p)\alpha$. We then optimize the constant coefficients α so the outputs of control law u best fit normative human joint torques y when inputting normative human kinematic trajectories [13].

The optimization problem is defined as

$$\begin{aligned}\arg\min_{\alpha} \quad & \textstyle\sum_j [U(q_j,p_j,\alpha) - Y_j]^T W_j [U(q_j,p_j,\alpha) - Y_j] \\ & + U(0,0,\alpha)^T W_r U(0,0,\alpha)\end{aligned}$$

where the objective function corresponds to the least square error of the exoskeleton control inputs $U \in \mathbb{R}^{m\times 1}$ and the normative human joint torques $Y_j \in \mathbb{R}^{m\times 1}$ with the weighting matrix W_j and the number of time samples m. The subscript j represents the number of different walking tasks, including level-ground walking and ramp walking. The state vectors $q_j, p_j \in \mathbb{R}^{m\times 1}$ comprise samples over time for the given task j. We also include W_r for regulation with zero states $q = 0$ and $p = 0$, where minimal torques should be provided.

A closed-form solution of the optimal coefficients α can be easily obtained as $\alpha^* = (\Phi^T W \Phi)^{-1}\Phi^T W Y$. As a result, the corresponding control law equals $u = \Phi(q,p)\alpha^*$, which will be scaled down to a desired fraction of normative torque.

E. Passivity and Stability

We now explore the input-output passivity and stability results of the exoskeleton-human system.

Proposition 2.2: The closed-loop system (2) is passive from the human input τ_{hum} to the output $\partial_p H$.

Proof: We can choose the total energy $E(q,p) = \tilde{H}$ as a storage function [17]. The time derivative of $E(q,p)$ is

$$\dot{E} = \nabla\tilde{H}^T \begin{bmatrix}\dot{q}\\ \dot{p}\end{bmatrix} = (\partial_p H)^T \tau_{\text{hum}} + (\partial_p H)^T A^T \tilde{\lambda} = (\partial_p H)^T \tau_{\text{hum}},$$

where we use the skew-symmetry property of the interconnection structure and $(\partial_p H)^T A^T \tilde{\lambda} = 0$ due to the fact that constraint forces do no work [18]. ■

Input-output passivity implies that the energy growth of the coupled human-exoskeleton system is controlled by the human. This provides safe interaction with the exoskeleton, but stability depends on the human control law. We examine stability of the closed-loop system around an equilibrium point in a similar way to [8]. The equilibrium point $(q^\star, 0)$ is the state where the forces along the shaped potential energy balance the muscular forces and the ground reaction forces, i.e., $X_\lambda \tilde{N} - X_\lambda \tau_{\text{hum}} = 0$. We make the common assumption that the human is modulating joint impedance where $\tau_{\text{hum}} = -K_p e - K_d \dot{e}$ [5]. The constant diagonal matrices K_p, K_d are positive semi-definite, and $e = q - \bar{q}$ represents the difference between q and the human's set-point vector $\bar{q}$ (which is not necessarily the same as the equilibrium $q^\star$ in impedance control). We can now state Proposition 2.3.

Proposition 2.3: Consider the closed-loop system (2), the equilibrium point $(q^\star, 0)$ is stable in the sense of Lyapunov given human input $\tau_{\text{hum}} = -K_p e - K_d \dot{e}$.

Proof: We can set the Lyapunov function to be

$$\mathscr{V}(q,p) = \tilde{H} + \frac{1}{2} e^T K_p e + \int_{q_0}^{q} A(s)^T \tilde{\lambda}(s,0) \cdot \mathrm{d}s - V^0, \tag{6}$$

where q_0 is the state at $t = 0$ and V^0 is a constant such that $\mathscr{V}$ is positive definite and vanishes at the equilibrium point $(q^\star, 0)$. The Lyapunov function $\mathscr{V}$ achieves its minimal point when $\partial_p \mathscr{V} = \dot{q} = p = 0$ and $\partial_q \mathscr{V} = \tilde{N} + K_p e + A^T \tilde{\lambda} = X_\lambda \tilde{N} - X_\lambda \tau_{\text{hum}} = 0$, i.e., at the equilibrium point $(q^\star, 0)$. The incorporation of $\int_{q_0}^{q} A(s)^T \tilde{\lambda}(s,0) \cdot ds$ guarantees the appearance of the GRFs to balance the unactuated parts of $\tilde{N}$ at the equilibrium state when $\partial_q \mathscr{V}(q,0) = 0$. As a result, the Lyapunov function $\mathscr{V}$ is positive definite and vanishes only at the equilibrium point $(q^\star, 0)$.

The time-derivative of Lyapunov function (6) is

$$\dot{\mathscr{V}} = \nabla\tilde{H}^T \begin{bmatrix}\dot{q}\\ \dot{p}\end{bmatrix} + \dot{q}^T K_p e + \dot{q}^T A^T \tilde{\lambda}(q,0) = -\dot{q}^T K_d \dot{q} \leq 0,$$

which shows that the shaped system is Lyapunov stable. ■

Although asymptotic stability has not been guaranteed, Lyapunov stability ensures the response will remain in a neighborhood of the equilibrium under human impedance control. This result satisfies our control objective of partial torque assistance while the human controls their kinematics.

III. Results

We now show optimization results to demonstrate the proposed controller's ability to recreate normative torques for three different ground slopes. We also experimentally implement the controller on a knee-ankle exoskeleton used by a healthy human subject as a proof-of-concept.

A. Design Optimization

The internal gyroscopic force term of the system includes centrifugal and Coriolis forces. Together with the gravitational vector N, these forces are expressed as trigonometric functions of state variables. As a result, we choose the basis functions in

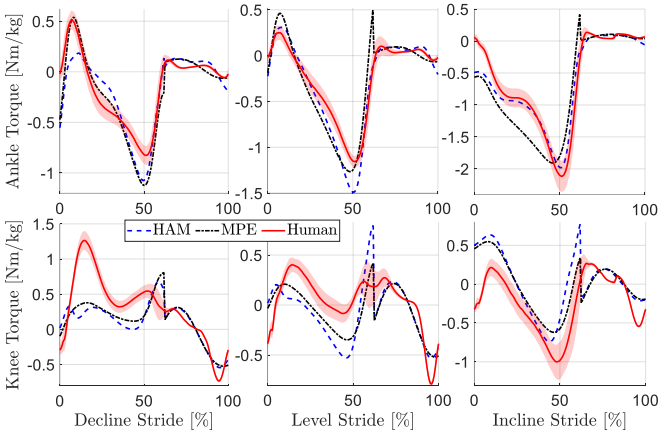

Fig. 3. Exoskeleton control torques and normative human torques (mean and variance) based on human treadmill walking data at incline (10°), level ground (0°), and decline (-10°) at 1m/s. Positive values represent ankle dorsiflexion and knee extension.

J_2 and $\hat{N}$ of the control law (5) to be trigonometric functions that depend on the actuated state variables (θ_a, θ_k), according to Proposition 2.1. We propose two shaping strategies: 1) modified potential energy (MPE) has basis functions for potential energy shaping only, and 2) modified Hamiltonian (HAM) has basis functions for artificial gyroscopic terms in addition to potential energy. The MPE method has six basis functions, and the HAM method has twelve basis functions (six more basis functions related to joint velocities). We fit the control law outputs to the across-subject averaged human joint moments over level-ground and slopes $\pm 10^\circ$ at a fixed walking speed (1m/s) [13]. The process provides the optimal parameters α. Fig. 3 shows the results with the derived control laws. The HAM method prevents the dorsiflexion spike at late stance exhibited by MPE during level and inclined walking. The HAM method also has a wider range for the knee torques due to the artificial gyroscopic terms, although they sometimes exceed normative trends (e.g., during late stance).

B. Proof-of-Concept Test with a Healthy Human Subject

1) Implementation: The controller was implemented on a 4.5 kg partial-assist knee-ankle exoskeleton (*Comex* [5], [19], Fig. 1) to demonstrate proof-of-concept for providing appropriate assistance over multiple walking conditions. The actuators are backdrivable due to a low 24:1 gear ratio, and produce 30 Nm continuous torque (60 Nm peak) using a 200 W frameless BLDC motor. Knee and ankle joint angles are provided by high-precision relative encoders. The commanded assistance torques are determined by multiplying the optimized control law (in Nm/kg) with the subject's body weight and a percent level-of-assistance.

2) Methods: As a proof-of-concept, we enrolled a single human subject (male, mass: 78 kg, height: 1.78 m) to demonstrate the controller's ability to assist musculature for multiple inclines and speeds. We consider different speeds to 1) check the controller's ability to handle extra conditions out of the design in Section III-A, and 2) investigate the effect of the velocity-dependent artificial gyroscopic terms of HAM method compared to the position-based MPE method. The study was approved by the Institutional Review Board at the University of Michigan (HUM00164931). We assessed muscle activation via electromyography (EMG) of vastus medialis oblique (VMO), biceps femoris (BF), tibialis anterior (TA), and soleus (SOL), which respectively function as a knee extensor, knee flexor, dorsiflexor, and plantarflexor.

The experiment consisted of four treadmill walking tasks: level walking at 0.6 m/s (cadence of 70 steps/min) and 1 m/s (cadence of 83 steps/min), and incline/decline walking on a $\pm 5^\circ$ slope at 0.6 m/s (cadence of 70 steps/min). The tasks were repeated for four exoskeleton modes: bare (no exoskeleton), passive (unpowered exoskeleton), active exoskeleton with MPE, and active exoskeleton with HAM. The speed (comfortable: 0.6 m/s, and fast: 1 m/s) and cadence were self-selected by the subject during practice trials and were encouraged with a metronome during the experimental trials. While a total of 30 gait cycles were collected for each task and mode, only the last 10 with relatively consistent kinematics were used for final analysis. Use of the treadmill handrails was disallowed during the experimental trials. The level-of-assistance for the active modes was set to 15%, based on the subject's comfort level during the practice trials.

The trials were cropped into gait cycles by using a threshold on the instrumented treadmill's vertical force. For each task, each muscle's EMG was rectified and smoothed using a second order low-pass Butterworth filter (cutoff 6 Hz), and then normalized with respect to the maximum peak of the ensemble averages (across repetitions) of the four modes as % MVC [20]. After temporally normalizing the EMG (as % stride), the mean amplitude was calculated to represent muscular effort, similar to [6].

3) Results: Table I presents muscular effort comparisons between the four modes for the four tasks. In general, the dominant muscles in the stance phase (VMO and SOL) had reduced effort for the active modes, compared to bare and especially passive. For VMO, this trend was the strongest for the decline task and held for the HAM mode's incline task. It should be noted that the VMO is significantly more active during the decline and incline tasks, compared to level walking [21], for which effort in active modes was reduced only compared to passive. Comex assistance reduced the SOL effort in the incline task, where it is considerably more active than level, and in decline where it is mostly passive [21]. Fig. 4 shows the ensemble-averaged VMO and SOL EMGs for bare and active modes, with the Comex assistance torques overlaid. Comex assistance torques were consistent with the optimized results in Fig. 3 and generally in harmony with the corresponding muscle activations for all tasks. One exception was during late stance-early swing, where the knee torque had an excessive peak. The general alignment explains the VMO and SOL effort reductions.

The active modes did not reduce muscle activation for TA and BF, which are mainly involved in the swing phase for leg clearance. Upon analysis of Fig. 4, we see that assistive dorsiflexion torques in the swing phase ($>60\%$ stride) were lower than the estimated backdrive torque (3 Nm, see [5, Fig. 16]), suggesting the subject experienced more resistance than assistance. Analysis of BF activity (not shown, similar trend to Fig. 4 in [6]) reveals large activity during late stance-early

TABLE I

EFFORT COMPARISONS FOR VMO, BF, TA, AND SOL: SHOWING MEAN (± SD) FOR TASKS (ROWS) AND MODES (COLUMNS).

	Effort [%MVC]	MPE	HAM	PASSIVE	BARE
Level 1.0 m/s	VMO	31.4 (2.1)	31.0 (2.1)	33.8 (2.0)	28.0 (3.3)
	BF	28.7 (3.5)	29.4 (4.2)	23.8 (3.1)	14.2 (1.9)
	TA	37.9 (3.9)	40.9 (1.4)	37.5 (1.5)	30.2 (5.7)
	SOL	26.3 (1.8)	27.5 (1.8)	31.8 (2.5)	25.1 (2.0)
Decline 0.6 m/s	VMO	35.4 (2.7)	33.3 (2.5)	43.1 (2.1)	49.4 (3.7)
	BF	35.6 (5.7)	32.6 (6.6)	37.6 (5.2)	26.9 (3.8)
	TA	31.4 (3.4)	32.8 (2.5)	32.9 (3.4)	18.7 (2.5)
	SOL	42.2 (5.7)	45.7 (5.7)	42.5 (6.5)	41.3 (3.4)
Level 0.6 m/s	VMO	34.9 (3.7)	35.8 (4.0)	39.4 (3.3)	35.9 (2.4)
	BF	24.2 (1.5)	25.2 (2.7)	22.8 (3.3)	10.9 (2.7)
	TA	29.7 (3.4)	30.7 (2.9)	27.0 (1.8)	18.5 (3.1)
	SOL	36.8 (5.0)	33.7 (3.4)	37.1 (4.2)	27.0 (3.3)
Incline 0.6 m/s	VMO	36.6 (3.9)	33.8 (2.7)	37.6 (3.3)	36.3 (7.0)
	BF	37.3 (5.3)	36.0 (6.2)	43.7 (4.5)	25.2 (3.8)
	TA	41.8 (8.3)	36.9 (2.4)	37.6 (4.0)	27.7 (6.1)
	SOL	25.7 (2.3)	29.2 (2.5)	29.3 (2.6)	31.2 (3.6)

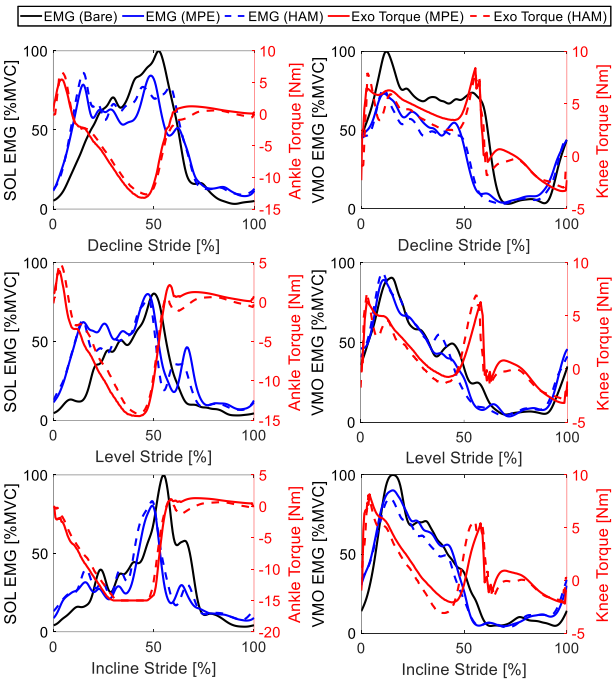

Fig. 4. SOL and VMO ensemble-averaged EMGs and respective Comex torques for decline (−5°), level (0°), and incline (5°) at 0.6 m/s. Positive torques represent ankle dorsiflexion and knee extension.

swing for both active and passive modes, compared to bare. This may be caused by the un-assisted hip joint compensating for the added distal mass of the exoskeleton, requiring greater hip drive (an additional function of the BF).

The observations in Fig. 4 and Table I meet our simulation expectations and demonstrate the potential to assist musculature in multiple tasks. Additional human subjects would be needed to draw more generic conclusions about the controller's effectiveness, which is left to future work.

IV. CONCLUSION

In this paper, we proposed a novel energetic control strategy for a knee-ankle exoskeleton that can shape both gravitational and gyroscopic terms based on the IDA-PBC, which was optimized to fit normative human torques. We performed a proof-of-concept experiment with an able-bodied human subject to demonstrate the proposed controller's ability to assist in multiple walking conditions. Future work will include more extensive clinical testing with this control approach. We will also extend the design optimization to include more tasks, including stair climbing and sit-to-stand/stand-to-sit.

REFERENCES

[1] T. Yan, M. Cempini, C. M. Oddo, and N. Vitiello, "Review of assistive strategies in powered lower-limb orthoses and exoskeletons," *Robot. Auton. Syst.*, vol. 64, pp. 120–136, 2015.

[2] O. Harib, A. Hereid, A. Agrawal, T. Gurriet, S. Finet, G. Boeris, A. Duburcq, M. E. Mungai, M. Masselin, A. D. Ames, K. Sreenath, and J. Grizzle, "Feedback control of an exoskeleton for paraplegics: Toward robustly stable, hands-free dynamic walking," *IEEE Control Syst. Mag.*, vol. 38, no. 6, pp. 61–87, 2018.

[3] G. Lv and R. D. Gregg, "Underactuated potential energy shaping with contact constraints: Application to a powered knee-ankle orthosis," *IEEE Trans. Control Syst. Technol.*, vol. 26, no. 1, pp. 181–193, 2018.

[4] A. M. Bloch, N. E. Leonard, and J. E. Marsden, "Stabilization of mechanical systems using controlled lagrangians," in *IEEE Conf. Decis. Control*, 1997, pp. 2356–2361.

[5] G. Lv, H. Zhu, and R. D. Gregg, "On the design and control of highly backdrivable lower-limb exoskeletons: A discussion of past and ongoing work," *IEEE Control Syst. Mag.*, vol. 38, no. 6, 2018.

[6] N. Divekar, J. Lin, C. Nesler, S. Borboa, and R. D. Gregg, "A potential energy shaping controller with ground reaction force feedback for a multi-activity knee-ankle exoskeleton," in *IEEE Int. Conf. Biomed. Robot. Biomechatronics*, 2020.

[7] J. Lin, G. Lv, and R. D. Gregg, "Contact-invariant total energy shaping control for powered exoskeletons," in *American Control Conf.* IEEE, 2019, pp. 664–670.

[8] J. Lin, N. Divekar, G. Lv, and R. D. Gregg, "Energy shaping control with virtual spring and damper for powered exoskeletons," in *IEEE Conf. Decis. Control*, 2019, pp. 3039–3045.

[9] J. E. Colgate and G. G. Schenkel, "Passivity of a class of sampled-data systems: Application to haptic interfaces," *J. Robot. Syst.*, vol. 14, no. 1, pp. 37–47, 1997.

[10] G. Blankenstein, R. Ortega, and A. J. Van Der Schaft, "The matching conditions of controlled lagrangians and ida-passivity based control," *Int. J. Control*, vol. 75, no. 9, pp. 645–665, 2002.

[11] R. Ortega, A. Van Der Schaft, B. Maschke, and G. Escobar, "Interconnection and damping assignment passivity-based control of port-controlled hamiltonian systems," *Automatica*, vol. 38, no. 4, 2002.

[12] V. de León-Gómez, V. Santibañez, and J. Sandoval, "Interconnection and damping assignment passivity-based control for a compass-like biped robot," *Int. J. Adv. Robot. Syst.*, vol. 14, no. 4, p. 1729881417716593, 2017.

[13] K. R. Embry, D. J. Villarreal, R. L. Macaluso, and R. D. Gregg, "Modeling the kinematics of human locomotion over continuously varying speeds and inclines," *IEEE Trans. Neural Syst. Rehabilitation Eng.*, vol. 26, no. 12, pp. 2342–2350, 2018.

[14] L. M. Mooney, E. J. Rouse, and H. M. Herr, "Autonomous exoskeleton reduces metabolic cost of human walking during load carriage," *J. Neuroeng. Rehabilitation*, vol. 11, no. 1, pp. 1–11, 2014.

[15] J. Wang, X. Li, T.-H. Huang, S. Yu, Y. Li, T. Chen, A. Carriero, M. Oh-Park, and H. Su, "Comfort-centered design of a lightweight and backdrivable knee exoskeleton," *IEEE Robot. Autom. Lett.*, vol. 3, no. 4, pp. 4265–4272, 2018.

[16] R. Ortega, A. Loría, P. J. Nicklasson, and H. J. Sira-Ramirez, *Passivity-based control of Euler-Lagrange systems*. Springer-Verlag, 1998.

[17] H. K. Khalil, *Nonlinear systems*. Upper Saddle River, NJ: Prentice Hall, 2002, vol. 3.

[18] R. M. Murray, *A mathematical introduction to robotic manipulation*. CRC press, 2017.

[19] H. Zhu, J. Doan, C. Stence, G. Lv, T. Elery, and R. Gregg, "Design and validation of a torque dense, highly backdrivable powered knee-ankle orthosis," in *IEEE Int. Conf. Robot. Autom.*, 2017, pp. 504–510.

[20] J. Yang and D. Winter, "Electromyographic amplitude normalization methods: improving their sensitivity as diagnostic tools in gait analysis," *Arch. Phys. Med. Rehabil.*, vol. 65, no. 9, p. 517—521, 1984.

[21] N. T. Pickle, A. M. Grabowski, A. G. Auyang, and A. K. Silverman, "The functional roles of muscles during sloped walking," *J. Biomechanics*, vol. 49, no. 14, pp. 3244–3251, 2016.